Journal of Materials Chemistry A

PAPER

View Article Online
View Journal | View Issue

Published on 14 April 2017. Downloaded by Synchrotron Radiation Library on 01/12/2017 03:40:44.

Check for updates

Cite this: J. Mater. Chem. A, 2017, 5, 9396

Electron acceptors with varied linkages between perylene diimide and benzotrithiophene for efficient fullerene-free solar cells†

Bo Wang,[a] Wenqing Liu,[a] Huanbin Li,[a] Jiangquan Mai,[b] Shiyong Liu,[a] Xinhui Lu,[b] Hanying Li,[a] Minmin Shi,[a] Chang-Zhi Li*[a] and Hongzheng Chen*[a]

Received 24th March 2017
Accepted 13th April 2017

DOI: 10.1039/c7ta02582c

rsc.li/materials-a

In this work, we present two new electron acceptors, TriPDI and Fused-TriPDI, in which three perylene diimide (PDI) moieties are tethered to a benzotrithiophene (BTT) core *via* either single bonds (TriPDI) or ring-fusion (Fused-TriPDI). TriPDI connects three PDIs to BTT *via* carbon–carbon single bonds, resulting in a rotatable and highly twisted skeleton. Instead, Fused-TriPDI, made through oxidative ring-fusion of TriPDI, exhibits good structural rigidity and planarity, as well as effective conjugation between PDI and BTT. As a result, the fused molecule shows up-shifted energy levels, and enhanced absorption and charge mobility over the unfused one. The polymer solar cells (PSCs) with a PTB7-Th:Fused-TriPDI blend show the best power conversion efficiency of 6.19%, which is around three times higher than that with PTB7-Th:TriPDI.

Introduction

Fullerene-free polymer solar cells (PSCs) have received a lot of attention recently, with high power conversion efficiencies (PCE) over 12%,[1–3] demonstrating the rivalry to those made with fullerene acceptors.[4–8] The structural flexibility in designing new nonfullerene acceptors offers advantages to materials with a wide range of optoelectronic tunabilities.[4,9–24] Among the reported nonfullerene acceptors, perylene diimide (PDI) is extensively employed due to its strong absorption and suitable energy levels.[25–38] On the other hand, one common observation is that the planar PDI aggregates severely in solids, which often leads to an unfavourable film morphology, and therefore the deteriorated PSC performance. To alleviate this issue, a strategy to engineer the topology of PDI acceptors into a nonplanar structure is developed to facilitate the appropriate phase separation with polymer electron donors.[14,26,27,39–47] Encouragingly, it has been shown that the fused PDI structure is effective in improving the performance of PDI acceptor-based PSCs.[12,25,28,30,35,48–50] In the fused structures, PDI units are bridged with the adjacent aromatics through six-membered rings. Consequently, they allow exhibiting good structural rigidity with the enhanced effective conjugation between PDI units, while still maintaining an overall non-planar molecular geometry.

However, a challenge involved in this effort is the difficulty to maintain the effective charge transport between nonplanar PDIs, which is likely due to the highly twisted molecule derived from the fusion of PDI to a congest core. It tends to decrease the intermolecular contact and orbital overlapping between PDI π-surfaces, where the lowest unoccupied molecular orbitals (LUMOs) are localized, thus hampering charge hopping between molecules. Therefore, to explore the new structural design of PDI is desirable, which can be conducive to improve the charge transport and phase separation of the PDI acceptor in bulk heterojunction (BHJ) blends, and ultimately beneficial for improving the PSC performance.

Herein we report the design and synthesis of two new nonfullerene electron acceptors, combining the extended benzotrithiophene (BTT) core with three PDI moieties. As shown in Scheme 1, TriPDI has three PDI moieties linked to BTT through carbon–carbon single bonds, resulting in a rotatable and highly twisted skeleton. After the oxidative ring-fusion of TriPDI, Fused-TriPDI is obtained that exhibits good structural rigidity and planarity, as well as the effective conjugation between PDI and BTT, in which PDI units are bridged with the adjacent BTT through six-membered rings. The introduction of electron-rich BTT to PDI can tune the energy level and absorption of molecules.

We further employ poly[4,8-bis(5-(2-ethylhexyl)thiophen-2-yl)benzo[1,2-*b*;4,5-*b*′]dithiophene-2,6-diyl-*alt*-(4-(2-ethylhexyl)-3-fluorothieno[3,4-*b*]thiophene)-2-carboxylate-2,6-diyl] (PTB7-Th) as the donor to fabricate PSCs, because of its complementary

[a]MOE Key Laboratory of Macromolecular Synthesis and Functionalization, State Key Laboratory of Silicon Materials, Department of Polymer Science and Engineering, Zhejiang University, Hangzhou 310027, P. R. China. E-mail: czli@zju.edu.cn; hzchen@zju.edu.cn

[b]Department of Physics, Chinese University of Hong Kong, New Territories, Hong Kong, P. R. China

† Electronic supplementary information (ESI) available. See DOI: 10.1039/c7ta02582c

This journal is © The Royal Society of Chemistry 2017

Published on 14 April 2017. Downloaded by Synchrotron Radiation Library on 01/12/2017 03:40:44.

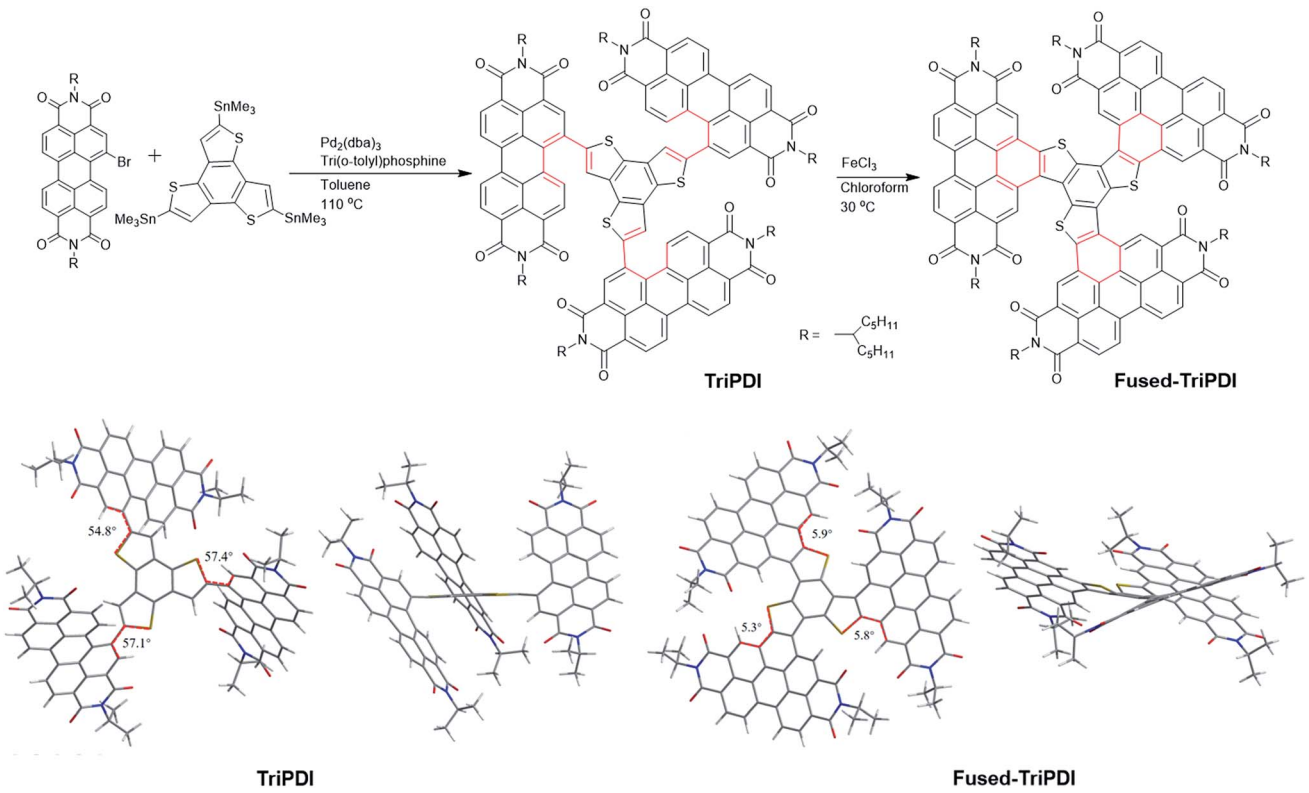

Scheme 1 Synthetic routes and chemical structures of TriPDI and Fused-TriPDI; views of the optimized geometries are obtained using DFT calculations at the B3LYP/6-31G(d) level.

absorption and energy level with TriPDI and Fused-TriPDI. The devices based on a PTB7-Th:Fused-TriPDI blend film exhibit the best PCE of 6.19%, which is almost three times higher than that with TriPDI (2.19%). The enhanced performance is mainly attributed to the increased electron mobility from Fused-TriPDI with the rigid and planar skeleton.

Results and discussion

Material synthesis and characterization

All reagents and solvents are purchased from commercial sources and used without further purification unless otherwise stated. *N*,*N*′-bis(6-hendecyl)perylene bismides and 5-bromo-*N*,*N*′-bis(6-hendecyl)perylene bismides are synthesized by following the reported literature.[51,52]

As shown in Scheme 1, Stille coupling between 5-bromo-*N*,*N*′-bis(6-hendecyl)perylene bismides and 2,5,8-tris(trimethylstannyl)benzo[1,2-*b*:3,4-*b*′:5,6-*b*″]trithiophene yields trilateral PDI (TriPDI). The final product is purified in a 65% yield. Fused trilateral PDI (Fused-TriPDI) is obtained in a yield of 82% through the oxidative cyclization with ferric chloride in chloroform. After purification by silica gel column chromatography, TriPDI and Fused-TriPDI are characterized by ^{1}H NMR (Fig. S1 and S2†), ^{13}C NMR, and mass spectra. Both TriPDI and Fused-TriPDI have good solubility in dichloromethane, chloroform, chlorobenzene, and dichlorobenzene. The thermal property was analysed by differential scanning calorimetry (DSC). As shown in Fig. S3,† there is no clear peak in DSC curves, indicative of the non-crystalline nature of both acceptors.

To compare the molecular geometry between TriPDI and Fused-TriPDI, density functional theory (DFT) calculations with B3LYP 6-31G base sets are carried out (ESI†), and the results are displayed in Scheme 1 and Fig. S4.† In TriPDI, each PDI unit is linked by BTT through single bonds. Owing to the steric effect and sp^3 hybrid carbon–carbon bond, TriPDI displays a highly twisted structure with a large dihedral angle over 50°. After ring-fusion, each PDI moiety is tethered to BTT through six-membered rings, resulting in the enhanced overall rigidity and planarity with small angles less than 6°.

The film and solution UV-vis absorption spectra of the two acceptors are shown in Fig. 1a and S5.† TriPDI in chloroform solution shows an intense absorption between 450 nm and

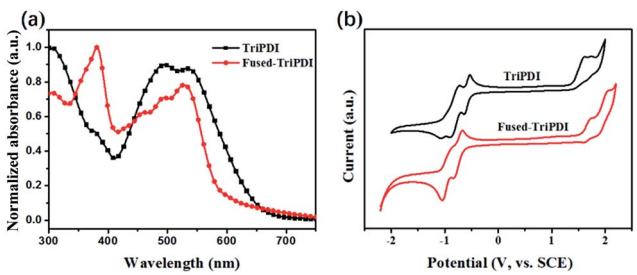

Fig. 1 (a) UV-vis absorption spectra of TriPDI and Fused-TriPDI in the film; (b) cyclic voltammograms of TriPDI and Fused-TriPDI.

Published on 14 April 2017. Downloaded by Synchrotron Radiation Library on 01/12/2017 03:40:44.

650 nm with a maximum extinction coefficient of 7.6×10^4 M^{-1} cm^{-1} at 502 nm. In a comparison, Fused-TriPDI shows stronger absorption between 340 nm and 600 nm with a maximum extinction coefficient of 9.9×10^4 M^{-1} cm^{-1} at 515 nm, which is in accord with the rigid Fused-TriPDI enhancing the effective conjugation between units, leading to the improved transition probability from the ground to the excited state.[53,54] Both TriPDI and Fused-TriPDI don't show obvious shift from the solution state to the film state, indicative of weak aggregation in the film state as expected.

As shown in Fig. 1a and S5,† the optical band gaps of TriPDI and Fused-TriPDI are estimated to be 1.99 eV and 2.20 eV, respectively. As shown in Fig. 1b, by using cyclic voltammetry (CV), LUMOs and the highest occupied molecular orbitals (HOMOs) are calculated to be −3.92/−5.80 eV (TriPDI) and −3.73/−5.95 eV (Fused-TriPDI). After ring-fusion, the fused structure delocalized the frontier orbitals, which weakens the intramolecular charge transfer between BTT and PDI moieties, thus leading to a wider band gap than that of TriPDI. As a result, Fused-TriPDI is expected to have an improved open-circuit voltage (V_{oc}) because of its upshifted LUMO energy level as an acceptor.

The charge mobility of TriPDI and Fused-TriPDI thin films spin-coated from $CHCl_3$ solution was measured in field-effect transistors (FETs) (bottom gate top contact). As shown in Fig. 2, the TriPDI device shows the best electron mobility of 1.26×10^{-4} cm^2 V^{-1} s^{-1}, while the Fused-TriPDI device shows an electron mobility of 1.26×10^{-3} cm^2 V^{-1} s^{-1}, nearly one order of magnitude higher than that of the unfused structure. The result indicates that Fused-TriPDI with improved structural rigidity and planarity has better intrinsic electron mobility than that of the twisted and rotatable TriPDI. Likely, Fused-TriPDI may possess a smaller reorganization energy than that of rotatable TriPDI, facilitating charge delocalization. In the meanwhile, the planar and extended structure of Fused-TriPDI easily promotes the intermolecular contact between PDI units, thus resulting in better electron mobility, which is close to that of fullerene bisadducts.[55]

Photovoltaic properties

To study the photovoltaic performance of TriPDI and Fused-TriPDI, both materials are used as electron acceptors to fabricate inverted devices with a configuration of ITO/ZnO/PTB7-Th:acceptor/MoO_3/Ag (see Fig. 3a). The energy levels of the active materials are provided in Fig. 3b. The current density–voltage (J–V) curves of the optimised devices are shown in Fig. 3c, and the photovoltaic parameters are summarized in Table 1. We varied the donor/acceptor (D/A) weight ratios from 1 : 1 to 1 : 2.5, and summarized the corresponding performance in Table S1.† The Fused-TriPDI device with a 1 : 1.5 blend ratio exhibits the best performance with a V_{oc} of 0.91 V, a short-circuit current density (J_{sc}) of 12.25 mA cm^{-2}, a fill factor (FF) of 0.52, and a PCE of 6.19%. As a comparison, the unfused TriPDI device with the same ratio shows the poor performance with a V_{oc} of 0.85 V, a J_{sc} of 6.13 mA cm^{-2}, a FF of 0.38, and a PCE of 2.14%. Solvent additives, such as 1-chloronaphthalene (CN), diphenyl ether (DPE) and 1,8-diiodooctane (DIO) are explored and the corresponding performances are listed in Table S2,† which indicate that additives have no positive effect in improving device performance based on the Fused-TriPDI acceptor.

External quantum efficiency (EQE) spectra are illustrated in Fig. 3d. Both of the blend films show photoresponses from 330 to 770 nm. The range of 330–580 nm is dominantly from the photocurrent contribution of a nonfullerene acceptor, and the range of 580–770 nm is from a PTB7-Th donor. The Fused-TriPDI device shows higher EQE intensities, which agree well with its increased J_{sc}.

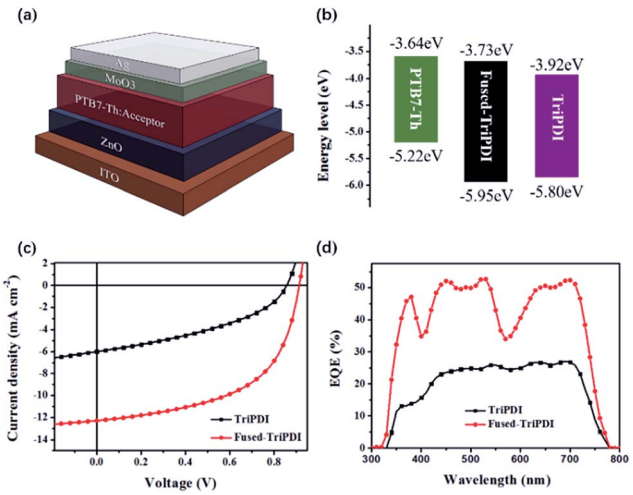

Fig. 3 (a) Diagram of a device structure; (b) energy levels of TriPDI, Fused-TriPDI and PTB7-Th; (c) J–V curves and (d) the corresponding EQE spectra of PTB7-Th:TriPDI and PTB7-Th:Fused-TriPDI-based PSCs.

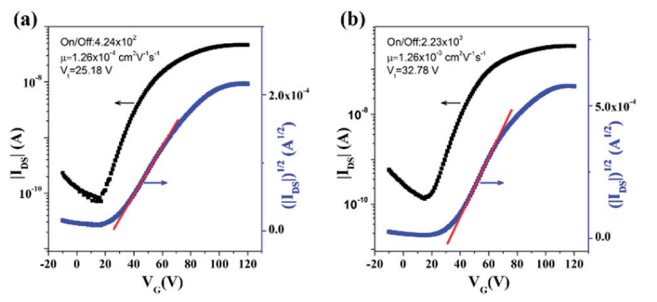

Fig. 2 FET characteristics of thin films spin-coated from $CHCl_3$ solutions: (a) TriPDI and (b) Fused-TriPDI.

Charge carrier mobility

To probe the charge transport in blend films, the hole and electron mobilities of the PTB7-Th:acceptor films were measured by the space-charge limited current (SCLC) method. The structure of the hole-only device is ITO/PEDOT:PSS/PTB7-Th:acceptor/MoO_3/Al, and the structure of the electron-only device is ITO/PFN/PTB7-Th:acceptor/PFN/Al. Fig. S6 and S7† show the $J^{0.5}$–V curves of the electron-only and hole-only devices, and Table 1 summarizes the mobility values calculated from the $J^{0.5}$–V curves using the Mott–Gurney law. The

 This journal is © The Royal Society of Chemistry 2017

Published on 14 April 2017. Downloaded by Synchrotron Radiation Library on 01/12/2017 03:40:44.

Table 1 Photovoltaic parameters of TriPDI and Fused-TriPDI-based PSCs

	D/A	V_{oc} (V)	J_{sc} (mA cm^{-2})	FF	PCE^b (%)	$\mu_{h\text{-SCLC}}$ (cm^2 V^{-1} s^{-1})	$\mu_{e\text{-SCLC}}$ (cm^2 V^{-1} s^{-1})	$\mu_{e\text{-FET}}$ (cm^2 V^{-1} s^{-1})
TriPDI	1 : 1.5^a	0.85	6.13	0.38	2.19 (2.14)	2.60×10^{-4}	2.52×10^{-4}	1.26×10^{-4}
Fused-TriPDI	1 : 1.5^a	0.91	12.39	0.55	6.19 (5.97)	4.17×10^{-4}	2.83×10^{-4}	1.26×10^{-3}

^{a} Annealing at 100 °C for 15 min. ^{b} Average PCE values obtained from 10 devices are shown in parentheses.

PTB7-Th:TriPDI blend film after annealing shows a hole mobility of 2.60×10^{-4} cm^2 V^{-1} s^{-1} and an electron mobility of 2.52×10^{-4} cm^2 V^{-1} s^{-1}. The PTB7-Th:Fused-TriPDI blend film after annealing shows a hole mobility of 4.17×10^{-4} cm^2 V^{-1} s^{-1} and an electron mobility of 2.83×10^{-4} cm^2 V^{-1} s^{-1}. Compared with TriPDI, Fused-TriPDI shows higher charge mobility, most likely due to the extended planar structure that is conducive to molecular contact and intramolecular electron delocalization. Besides this, the electron mobility of Fused-TriPDI in the horizontal direction also shows one order of magnitude higher than that of TriPDI in FET measurements. These factors combined together may be responsible for the higher J_{sc}, FF, and EQE in the PSCs employing the fused structure.

Morphology characterization

To understand the reason for performance variation in PSCs, the morphology of PTB7-Th:acceptor blends is investigated. Grazing incidence wide-angle X-ray scattering (GIWAXS) was employed to investigate the crystallinity and molecular packing of the active layers.[56] The 2D GIWAXS patterns and the corresponding out-of-plane and in-plane intensity profiles are shown in Fig. S8† and Fig. 4.

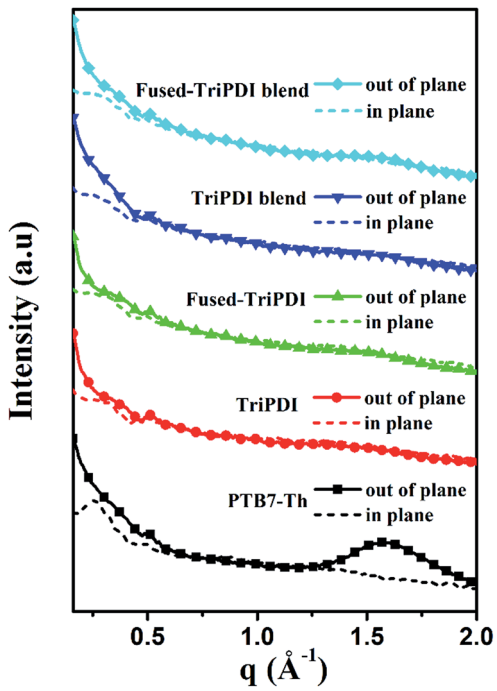

Fig. 4 GIWAXS scattering profiles and the in-plane (dashed line) and out-of-plane (solid line) profiles of neat PTB7-Th, neat TriPDI, neat Fused-TriPDI, and the blends (D:A = 1 : 1.5, w/w).

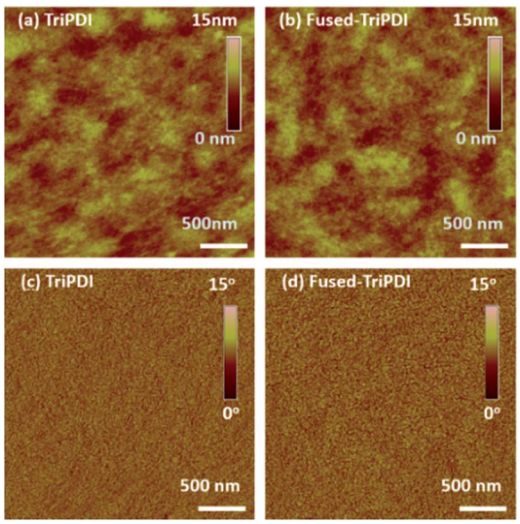

Fig. 5 AFM height (a and b) and phase (c and d) images of PTB7-Th:acceptor (1 : 1.5, w/w) blend films.

The neat PTB7-Th film shows a lamellar stacking (100) diffraction peak in the in-plane direction at 0.26 Å^{-1} and a π–π stacking (010) diffraction peak in the out-of-plane direction at 1.58 Å^{-1}, corresponding to a lattice constant of 2.42 nm and 0.40 nm, respectively. In the out-of-plane direction, there is no obvious diffraction peak observed in the neat TriPDI film or Fused-TriPDI film. And the PTB7-Th:TriPDI and PTB7-Th:Fused-TriPDI blends show a weak (010) diffraction peak at ~1.58 Å^{-1}. In the in-plane direction, compared with the neat TriPDI film and the PTB7-Th:TriPDI blended film, the neat Fused-TriPDI film shows a stronger diffraction intensity at 0.26 Å^{-1} of lamellar stacking. These data indicate that the PTB7-Th:Fused-TriPDI blended film has a preferred face-on orientation, which confirms the improved SCLC charge mobility.

As shown in Fig. 5, the atomic force microscopy (AFM) images of the PBT7:TriPDI film suggest a smooth surface with a root mean square (RMS) roughness of 1.04 nm. The PBT7:Fused-TriPDI blend film shows a similar smooth surface with a RMS of 1.02 nm. The smooth surface indicates the good miscibility of PTB7 and the acceptors.

Conclusions

In summary, two new electron acceptors, TriPDI and Fused-TriPDI are designed and synthesised by using PDI moieties

Published on 14 April 2017. Downloaded by Synchrotron Radiation Library on 01/12/2017 03:40:44.

and a BTT core. Through the oxidative ring-fusion of TriPDI with singly bonded PDIs to BTT, Fused-TriPDI exhibits improved structural rigidity and planarity, as well as effective conjugation between PDI and BTT. It has been revealed that the fused molecule shows not only up-shifted energy levels and enhanced absorption, but also improved charge mobility over the unfused one. As a result, the PSCs with the PTB7-Th:Fused-TriPDI blend show a power conversion efficiency of 6.19%, almost three times higher than that with PTB7-Th:TriPDI. This work demonstrates a successful example of constructing a fused PDI structure with an extended core to improve fullerene-free PSC performance.

Acknowledgements

This research was funded by the National Natural Science Foundation of China (No. 21674093 and 51620105006), 973 program (No. 2014CB643503) and the International Science and Technology Cooperation Program of China (ISTCP) (Grant No. 2016YFE0102900). C.-Z. Li thanks the support by the Zhejiang Natural Science Fund for Distinguished Young Scholars (LR17E030001), the Young 1000 Talents Global Recruitment Program of China, and 100 Talents Program of Zhejiang University. J. Mai and X. Lu gratefully thank the beam time and technical supports provided by 23A SWAXS beamline at NSRRC, Hsinchu.

Notes and references

1 F. Zhao, S. Dai, Y. Wu, Q. Zhang, J. Wang, L. Jiang, Q. Ling, Z. Wei, W. Ma, W. You, C. Wang and X. Zhan, *Adv. Mater.*, 2017, 1700144, DOI: 10.1002/adma.201700144.
2 W. Zhao, S. Li, S. Zhang, X. Liu and J. Hou, *Adv. Mater.*, 2017, **29**, 1604059.
3 S. Li, L. Ye, W. Zhao, S. Zhang, S. Mukherjee, H. Ade and J. Hou, *Adv. Mater.*, 2016, **28**, 9423–9429.
4 J. Zhao, Y. Li, G. Yang, K. Jiang, H. Lin, H. Ade, W. Ma and H. Yan, *Nat. Energy*, 2016, **1**, 15027.
5 C.-Z. Li, H.-L. Yip and A. K. Y. Jen, *J. Mater. Chem.*, 2012, **22**, 4161–4177.
6 J. Huang, X. Zhang, D. Zheng, K. Yan, C.-Z. Li and J. Yu, *Solar RRL*, 2017, **1**, 1600008.
7 J. Huang, H. Wang, K. Yan, X. Zhang, H. Chen, C.-Z. Li and J. Yu, *Adv. Mater.*, 2017, 1606729, DOI: 10.1002/adma.201606729.
8 T. Kumari, S. M. Lee, S.-H. Kang, S. Chen and C. Yang, *Energy Environ. Sci.*, 2017, **10**, 258–265.
9 C. B. Nielsen, S. Holliday, H.-Y. Chen, S. J. Cryer and I. McCulloch, *Acc. Chem. Res.*, 2015, **48**, 2803–2812.
10 Y. Lin, Q. He, F. Zhao, L. Huo, J. Mai, X. Lu, C. J. Su, T. Li, J. Wang, J. Zhu, Y. Sun, C. Wang and X. Zhan, *J. Am. Chem. Soc.*, 2016, **138**, 2973–2976.
11 C. Zhan, X. Zhang and J. Yao, *RSC Adv.*, 2015, **5**, 93002–93026.
12 S. Holliday, R. S. Ashraf, A. Wadsworth, D. Baran, S. A. Yousaf, C. B. Nielsen, C. H. Tan, S. D. Dimitrov, Z. Shang, N. Gasparini, M. Alamoudi, F. Laquai, C. J. Brabec, A. Salleo, J. R. Durrant and I. McCulloch, *Nat. Commun.*, 2016, **7**, 11585.
13 S. Badgujar, C. E. Song, S. Oh, W. S. Shin, S.-J. Moon, J.-C. Lee, I. H. Jung and S. K. Lee, *J. Mater. Chem. A*, 2016, **4**, 16335–16340.
14 N. Liang, K. Sun, Z. Zheng, H. Yao, G. Gao, X. Meng, Z. Wang, W. Ma and J. Hou, *Adv. Energy Mater.*, 2016, **6**, 1600060.
15 S. Dai, F. Zhao, Q. Zhang, T.-K. Lau, T. Li, K. Liu, Q. Ling, C. Wang, X. Lu, W. You and X. Zhan, *J. Am. Chem. Soc.*, 2017, **139**, 1336–1343.
16 H. Yao, Y. Cui, R. Yu, B. Gao, H. Zhang and J. Hou, *Angew. Chem., Int. Ed.*, 2017, **56**, 3045–3049.
17 L. Zhong, L. Gao, H. Bin, Q. Hu, Z.-G. Zhang, F. Liu, T. P. Russell, Z. Zhang and Y. Li, *Adv. Energy Mater.*, 2017, 1602215, DOI: 10.1002/aenm.201602215.
18 S. Li, Z. Zhang, M. Shi, C.-Z. Li and H. Chen, *Phys. Chem. Chem. Phys.*, 2017, **19**, 3440–3458.
19 W. Zhao, D. Qian, S. Zhang, S. Li, O. Inganas, F. Gao and J. Hou, *Adv. Mater.*, 2016, **28**, 4734–4739.
20 H. Bin, Z. G. Zhang, L. Gao, S. Chen, L. Zhong, L. Xue, C. Yang and Y. Li, *J. Am. Chem. Soc.*, 2016, **138**, 4657–4664.
21 F. Liu, Z. Zhou, C. Zhang, T. Vergote, H. Fan, F. Liu and X. Zhu, *J. Am. Chem. Soc.*, 2016, **138**, 15523–15526.
22 X. Long, Z. Ding, C. Dou, J. Zhang, J. Liu and L. Wang, *Adv. Mater.*, 2016, **28**, 6504–6508.
23 Y. Lin, F. Zhao, Q. He, L. Huo, Y. Wu, T. C. Parker, W. Ma, Y. Sun, C. Wang, D. Zhu, A. J. Heeger, S. R. Marder and X. Zhan, *J. Am. Chem. Soc.*, 2016, **138**, 4955–4961.
24 S. Li, W. Liu, M. Shi, J. Mai, T.-K. Lau, J. Wan, X. Lu, C.-Z. Li and H. Chen, *Energy Environ. Sci.*, 2016, **9**, 604–610.
25 H. Zhong, C. H. Wu, C. Z. Li, J. Carpenter, C. C. Chueh, J. Y. Chen, H. Ade and A. K. Jen, *Adv. Mater.*, 2016, **28**, 951–958.
26 D. Sun, D. Meng, Y. Cai, B. Fan, Y. Li, W. Jiang, L. Huo, Y. Sun and Z. Wang, *J. Am. Chem. Soc.*, 2015, **137**, 11156–11162.
27 Y. Zhong, M. T. Trinh, R. Chen, W. Wang, P. P. Khlyabich, B. Kumar, Q. Xu, C. Y. Nam, M. Y. Sfeir, C. Black, M. L. Steigerwald, Y. L. Loo, S. Xiao, F. Ng, X. Y. Zhu and C. Nuckolls, *J. Am. Chem. Soc.*, 2014, **136**, 15215–15221.
28 Y. Zhong, B. Kumar, S. Oh, M. T. Trinh, Y. Wu, K. Elbert, P. Li, X. Zhu, S. Xiao, F. Ng, M. L. Steigerwald and C. Nuckolls, *J. Am. Chem. Soc.*, 2014, **136**, 8122–8130.
29 D. Zhao, Q. Wu, Z. Cai, T. Zheng, W. Chen, J. Lu and L. Yu, *Chem. Mater.*, 2016, **28**, 1139–1146.
30 D. Meng, H. Fu, C. Xiao, X. Meng, T. Winands, W. Ma, W. Wei, B. Fan, L. Huo, N. L. Doltsinis, Y. Li, Y. Sun and Z. Wang, *J. Am. Chem. Soc.*, 2016, **138**, 10184–10190.
31 A. D. Hendsbee, J.-P. Sun, W. K. Law, H. Yan, I. G. Hill, D. M. Spasyuk and G. C. Welch, *Chem. Mater.*, 2016, **28**, 7098–7109.
32 T. Liu, D. Meng, Y. Cai, X. Sun, Y. Li, L. Huo, F. Liu, Z. Wang, T. P. Russell and Y. Sun, *Adv. Sci.*, 2016, **3**, 1600117.
33 X. Liu, T. Liu, C. Duan, J. Wang, S. Pang, W. Xiong, Y. Sun, F. Huang and Y. Cao, *J. Mater. Chem. A*, 2017, **5**, 1713–1723.
34 F. Fernandez-Lazaro, N. Zink-Lorre and A. Sastre-Santos, *J. Mater. Chem. A*, 2016, **4**, 9336–9346.

 This journal is © The Royal Society of Chemistry 2017

Published on 14 April 2017. Downloaded by Synchrotron Radiation Library on 01/12/2017 03:40:44.

35 Y. Zhong, M. T. Trinh, R. Chen, G. E. Purdum, P. P. Khlyabich, M. Sezen, S. Oh, H. Zhu, B. Fowler, B. Zhang, W. Wang, C. Y. Nam, M. Y. Sfeir, C. T. Black, M. L. Steigerwald, Y. L. Loo, F. Ng, X. Y. Zhu and C. Nuckolls, *Nat. Commun.*, 2015, **6**, 8242.
36 A. Zhang, C. Li, F. Yang, J. Zhang, Z. Wang, Z. Wei and W. Li, *Angew. Chem., Int. Ed.*, 2017, **56**, 2694–2698.
37 W. Chen and Q. Zhang, *J. Mater. Chem. C*, 2017, **5**, 1275–1302.
38 S. Chen, G. Zhang, J. Liu, H. Yao, J. Zhang, T. Ma, Z. Li and H. Yan, *Adv. Mater.*, 2017, **29**, 1604231.
39 Y. Zang, C. Z. Li, C. C. Chueh, S. T. Williams, W. Jiang, Z. H. Wang, J. S. Yu and A. K. Jen, *Adv. Mater.*, 2014, **26**, 5708–5714.
40 C.-H. Wu, C.-C. Chueh, Y.-Y. Xi, H.-L. Zhong, G.-P. Gao, Z.-H. Wang, L. D. Pozzo, T.-C. Wen and A. K. Y. Jen, *Adv. Funct. Mater.*, 2015, **25**, 5326–5332.
41 S. Li, W. Liu, C.-Z. Li, F. Liu, Y. Zhang, M. Shi, H. Chen and T. P. Russell, *J. Mater. Chem. A*, 2016, **4**, 10659–10665.
42 J. Zhao, Y. Li, H. Lin, Y. Liu, K. Jiang, C. Mu, T. Ma, J. Y. Lin Lai, H. Hu, D. Yu and H. Yan, *Energy Environ. Sci.*, 2015, **8**, 520–525.
43 D. Meng, D. Sun, C. Zhong, T. Liu, B. Fan, L. Huo, Y. Li, W. Jiang, H. Choi, T. Kim, J. Y. Kim, Y. Sun, Z. Wang and A. J. Heeger, *J. Am. Chem. Soc.*, 2016, **138**, 375–380.
44 J. Lee, R. Singh, D. H. Sin, H. G. Kim, K. C. Song and K. Cho, *Adv. Mater.*, 2016, **28**, 69–76.
45 S.-Y. Liu, C.-H. Wu, C.-Z. Li, S.-Q. Liu, K.-H. Wei, H.-Z. Chen and A. K. Y. Jen, *Adv. Sci.*, 2015, **2**, 1500014.
46 Y. Duan, X. Xu, H. Yan, W. Wu, Z. Li and Q. Peng, *Adv. Mater.*, 2017, **29**, 1605115.
47 W. Chen, X. Yang, G. Long, X. Wan, Y. Chen and Q. Zhang, *J. Mater. Chem. C*, 2015, **3**, 4698–4705.
48 H. Fu, D. Meng, X. Meng, X. Sun, L. Huo, Y. Fan, Y. Li, W. Ma, Y. Sun and Z. Wang, *J. Mater. Chem. A*, 2017, **5**, 3475–3482.
49 N. Liang, D. Meng, Z. Ma, B. Kan, X. Meng, Z. Zheng, W. Jiang, Y. Li, X. Wan, J. Hou, W. Ma, Y. Chen and Z. Wang, *Adv. Energy Mater.*, 2016, 1601664, DOI: 10.1002/aenm.201601664.
50 S. Li, J. Yan, C.-Z. Li, F. Liu, M. Shi, H. Chen and T. P. Russell, *J. Mater. Chem. A*, 2016, **4**, 3777–3783.
51 Y. Huang, J. Hu, W. Kuang, Z. Wei and C. F. J. Faul, *Chem. Commun.*, 2011, **47**, 5554–5556.
52 Y. Yang, Y. Wang, Y. Xie, T. Xiong, Z. Yuan, Y. Zhang, S. Qian and Y. Xiao, *Chem. Commun.*, 2011, **47**, 10749–10751.
53 S. Ko, R. Mondal, C. Risko, J. K. Lee, S. Hong, M. D. McGehee, J.-L. Brédas and Z. Bao, *Macromolecules*, 2010, **43**, 6685–6698.
54 R. Mondal, S. Ko, J. E. Norton, N. Miyaki, H. A. Becerril, E. Verploegen, M. F. Toney, J.-L. Bredas, M. D. McGehee and Z. Bao, *J. Mater. Chem.*, 2009, **19**, 7195–7197.
55 C.-Z. Li, C.-C. Chueh, H.-L. Yip, J. Zou, W.-C. Chen and A. K. Y. Jen, *J. Mater. Chem.*, 2012, **22**, 14976–14981.
56 J. Mai, T.-K. Lau, J. Li, S.-H. Peng, C.-S. Hsu, U. S. Jeng, J. Zeng, N. Zhao, X. Xiao and X. Lu, *Chem. Mater.*, 2016, **28**, 6186–6195.